Reflectivity of Metals in the Millimeter Wavelength Range at Cryogenic Temperatures

Evgeny A. Serov, Vladimir V. Parshin, and Grigoriy M. Bubnov

***Abstract*— We present the results of theoretical and experimental studies of the reflectivity of metals at cryogenic temperatures in the millimeter wavelength range. High-Q Fabry–Perot resonators operated at a temperature of 4–300 K in the frequency range 150–250 GHz are used for the experimental study. Silver, copper, gold, aluminum, and beryllium reflectors with different structures are examined. It has been shown that the reflection loss at cryogenic temperatures varies considerably (several times) depending on the structure of the sample surface and the presence of impurities. The obtained data make it possible to calculate the thermal noise of cooled reflectors of the antenna systems in millimeter and submillimeter telescopes.**

***Index Terms*— Anomalous skin effect, antenna reflectors, Fabry–Perot resonator, millimeter (mm) and submillimeter (sub-mm) waves, reflectivity of metals, surface resistance.**

I. Introduction

AT PRESENT, there is intense development of the technique in the millimeter (mm) and submillimeter (sub-mm) ranges by industry. In particular, the frequency range of 45–500 GHz is used for wireless transmission of large amounts of data [1], remote sensing of the environment [2], radio astronomical observations, and for other tasks. Despite the intense development of the technologies in these ranges, many characteristics of the materials remain poorly studied. One of such characteristics is the reflectivity of metals cooled to cryogenic temperatures. The studies of reflectivity at cryogenic temperatures are mostly required for the construction of satellite-borne and ground-based millimeter and submillimeter telescopes with highly sensitive receivers cooled to 0.1 K by Helium-III (Planck, Herschel, and Millimetron projects). In this case, the energy loss by reflection in the antenna reflector system (reflection loss), or, in other words, its thermal radiation, increases uncontrollably the noise temperature of the receiver module. To reduce the noise temperature of the receiver module, the entire antenna system for the Millimetron project (main mirror and all the antenna line) are expected to be cooled to temperatures of about 4 K [3]. Important information for calculation of the sensitivity of such a complex, besides the intrinsic noise temperature of the receiver, is the reflection loss, i.e., the emission coefficient of the antenna system reflectors in the specified frequency range and at a given temperature. The need for precise determination of antenna system reflectivity is due to high demands on the instrument sensitivity. For example, the Planck project required the ability to detect the anisotropy of the background cosmic radiation at the level 10^{-6} K [4]. The requirements for the new project COrE are even higher [5]. An important research area is measuring the metal coating reflectivity of composite materials. Typically, large-diameter antennas are made of carbon fiber-reinforced plastic with the reflective metal film applied on its surface [4]. The previous studies [6]–[8] have shown that the reflection loss of such composite materials can differ significantly (several times) from calculated values. The findings contributed to the adoption of the concept that all the Millimetron reflectors should be covered by a layer of gold with a thickness of several skin depths to reduce the reflection loss and ensure good repeatability of measurements.

Calculation of the metal reflectivity can be made on the basis of the skin effect theory. At cryogenic temperatures, the so-called anomalous skin effect takes place [9], [10]. The method of theoretical calculation of the reflectance having regard to the anomalous skin effect has been known for a long time [11], [12]. However, the accuracy of such calculation is not sufficient for the real samples with impurities and defects of the surface structure. The formula for the reflectivity calculation may include a lot of parameters that are not known *a priori*. For example, the presence of even a small amount of impurities may significantly (several times) increase the reflection loss at liquid helium temperatures [8]. Therefore, reliable experimental data on the metal reflectivity in a wide temperature range are very valuable for practical applications. In our previous publications [6]–[8], [13], one can find brief information about reflection loss measurements and the data obtained using a high-sensitivity resonator technique. In this paper, we present a detailed description of the experimental technique and method, new experimental results, their analysis and interpretation.

Section II presents the results of theoretical calculations of the metal reflectivity and discusses the limitations of using such calculations for real samples. Section III describes the experimental setup and the method for a study of the sample reflectivity. Section IV presents the experimental results. Section V is devoted to the calculation of the contribution of the thermal radiation of the reflectors to the noise temperature of the receiver. Section VI contains the conclusions.

II. Metal Reflectivity Calculation

When a metal interacts with an electromagnetic wave, a skin effect, i.e., penetration of the electromagnetic field into the

Manuscript received February 25, 2016; revised April 26, 2016 and August 24, 2016; accepted August 25, 2016. Date of publication September 29, 2016; date of current version November 3, 2016. This work was supported in part by the President of the Russian Federation for the support of young scientists under Grant MK-6696.2015.2.

The authors are with the Institute of Applied Physics, Russian Academy of Sciences, 603950 Nizhny Novgorod, Russia (e-mail: serov@ipfran.ru; parsh@appl.sci-nnov.ru; payalnik89@gmail.com).

Color versions of one or more of the figures in this paper are available online at http://ieeexplore.ieee.org.

Digital Object Identifier 10.1109/TMTT.2016.2609411

metal to a depth called the skin-layer depth δ, takes place. The value of δ for each metal is a function of the frequency and temperature.

Confining ourselves to the mm and submillimeter ranges, we can talk about two limiting cases of such a dependence, namely, the normal skin effect and the extremely anomalous skin effect. Let l be the mean free path of the conduction electrons in a metal. Then the normal skin effect takes place under the condition $l \ll \delta$, and the extremely anomalous skin effect takes place under the inverse condition $l \gg \delta$. In the first case, the metal can be considered as a medium with complex dielectric permittivity

$$\varepsilon(\omega) = (4\pi\sigma/\omega) \cdot i \tag{1}$$

where σ is the dc conductance of the metal, $\omega = 2\pi f$, f is the frequency of the electromagnetic wave, and i is the imaginary unit. The power reflectance for the case of the normal incidence can be expressed via ε using the formula

$$R = \left|\frac{\sqrt{\varepsilon}-1}{\sqrt{\varepsilon}+1}\right|^2. \tag{2}$$

Taking into account (1) and assuming $\sigma \gg \omega$, we obtain the Hagen–Rubens formula for the reflectance of a metal

$$R = 1 - 2\sqrt{f/\sigma} = 1 - 2k_0\delta. \tag{3}$$

Here, $k_0 = \omega/c$, where c is the speed of light. The depth of the skin layer is expressed as follows:

$$\delta = c/\sqrt{2\pi\sigma\omega}. \tag{4}$$

The behavior of most of the metals at room temperature is described by (3) and (4). However, when metals are cooled to liquid-nitrogen or lower temperatures and the skin-layer depth δ becomes close to the electron's free path l, this approximation is no longer valid. The connection between the current density $\vec{j}$ and the field $\vec{E}$ in a metal ceases to be local. To find this connection, it is necessary to solve the kinetic equation for the distribution function w of electrons in a metal [10]

$$\frac{\partial w}{\partial t} + \vec{v}\frac{\partial w}{\partial \vec{r}} - e\vec{E}\frac{\partial w}{\partial \vec{p}} = St\{w\} \tag{5}$$

where $\vec{v}$ is the electron velocity, $\vec{p}$ is the electron momentum, e is the elementary charge, and $St\{w\}$ is the collision integral. If the distribution function $w\ (\vec{p}, \vec{r})$ is known, then the current density can be calculated using the formula [10]

$$\vec{j} = -\frac{2e}{(2\pi\hbar)^3}\int \vec{v}(\vec{p})w(\vec{p},\vec{r})d^3p. \tag{6}$$

Electromagnetic fields and currents in a metal obey the Maxwell quasi-stationary equations (the case of monochromatic fields for the magnetic permeability $\mu = 1$, with the bias current neglected)

$$\begin{cases} \text{rot } \vec{E} = \dfrac{i\omega}{c}\vec{H} \\ \text{rot } \vec{H} = \dfrac{4\pi}{c}\vec{j}. \end{cases} \tag{7}$$

We now define the concept of the surface impedance of a metal. We introduce the coordinate system in such a way that the metal surface coincides with the (x, y) plane and the z-axis is directed into the metal interior (Fig. 1). Let a plane wave be incident on the metal perpendicular to its surface, and the field $\vec{E}$ have only the x component (this can be assumed without loss of generality for an isotropic metal). Then the surface impedance of the metal is given by $\xi = ((E_x)/(H_y))|_{z=0}$. In the case of the normal skin effect, we have $\xi = (1/\sqrt{\varepsilon})$, and (2) can therefore be written in another form

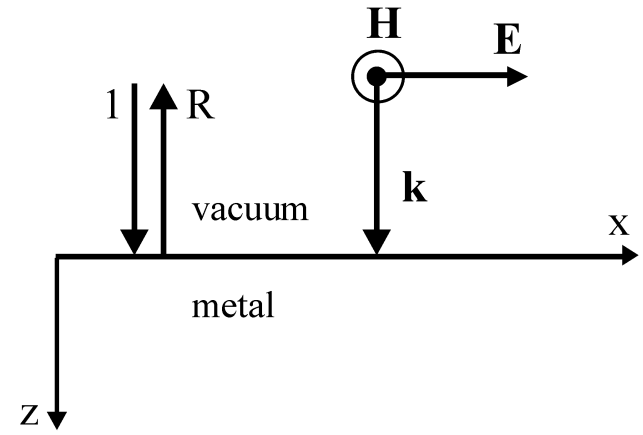

Fig. 1. Scheme of normal incidence of a plane electromagnetic wave on the metal layer.

$$R = \left|\frac{1/\xi - 1}{1/\xi + 1}\right|^2. \tag{8}$$

It can be shown that (8) holds for any character of the skin effect and can therefore be used to calculate the reflectance at an arbitrary temperature [14]. Thus, to find the reflectance, it is generally necessary to solve (5) and (7) jointly with (6) and to express the surface impedance. Usually, in the literature, the limiting case $l \gg \delta$ is considered in detail and a formula for calculation of ξ for a metal with arbitrary shape of the Fermi surface is given [9]. To study the temperature dependence of the reflectance of isotropic metals, it seems more interesting to calculate ξ for an arbitrary ratio of l and δ, assuming that the Fermi surface is spherical to a first approximation.

To solve the kinetic equation, we use the first-order perturbation theory, $w = w_0 + w_1$, where w_0 is the unperturbed distribution function and w_1 is a perturbation proportional to the field $\vec{E}$. We assume that a formula given by $St\{w\} = -((w - w_0)/\tau)$, where τ is the electron's mean free path time, applies for the collision integral. Then, assuming $w_1(\vec{v}, z, t) = W_1(\vec{v}, z) \cdot \exp(-i\omega t)$, we obtain

$$\frac{1}{\tau_1}W_1 + v_z\frac{\partial W_1}{\partial z} = eE_\beta\frac{\partial w_0}{\partial p_\beta} \tag{9}$$

where $\tau_1 = (\tau/(1 - i\omega\tau))$, $\beta = x, y$. General solution of (9) with allowance for the equality $((\partial w_0)/(\partial p_\beta)) = v_\beta((\partial w_0)/(\partial \varepsilon_e))$, where ε_e is the electron energy, can be written in the form

$$W_1 = \frac{e}{v_z}\frac{\partial w_0}{\partial \varepsilon_e}\exp\left(-\frac{z}{v_z\tau_1}\right) \cdot \left(\int_0^z v_\beta E_\beta(\zeta)\exp\left(\frac{\zeta}{v_z\tau_1}\right)d\zeta + A(\vec{v})\right) \tag{10}$$

where $A(\vec{v})$ is an arbitrary function of velocity. To find $A(\vec{v})$, it is needed to use the boundary conditions for $z = 0$ and $z = +\infty$. The case where the boundary condition on the metal surface corresponds to the specular reflectance of electrons

$$W_1(p_z, z = 0) = W_1(-p_z, z = 0) \tag{11}$$

is the simplest for the analysis. Another form of the boundary condition is the diffuse reflection of electrons

$$W_1(p_z < 0, z = 0) = 0. \tag{12}$$

For the diffuse reflection of electrons, the surface impedance calculation is a more complicated problem, but the final result of the surface impedance calculation in the case of an extremely anomalous skin layer is different by less than 10% [9]. Therefore, we confine ourselves to considering condition (11). In view of the second boundary condition $W_1(z = +\infty) = 0$, the following expression can be obtained for the components of the current density:

$$j_\alpha = -\frac{2e}{(2\pi\hbar)^3}\int_{v_z>0}\frac{\partial w_0}{\partial \varepsilon_e} \times \left\{\begin{array}{l} \displaystyle\int_0^z \frac{v_\alpha v_\beta}{v_z} E_\beta(\zeta)\exp\left(-\frac{z-\zeta}{v_z\tau_1}\right)d\zeta + \\ \displaystyle + \int_0^\infty \frac{v_\alpha v_\beta}{v_z} E_\beta(\zeta)\exp\left(-\frac{z+\zeta}{v_z\tau_1}\right)d\zeta + \\ \displaystyle + \int_z^\infty \frac{v_\alpha v_\beta}{v_z} E_\beta(\zeta)\exp\left(\frac{z-\zeta}{v_z\tau_1}\right)d\zeta \end{array}\right\} d^3p.$$

Integration over ζ is performed inside the metal. However, if we assume that the electric field is continued symmetrically outside the metal, then the expression for the current density will take the form

$$j_\alpha(z) = \int_{-\infty}^{\infty} K_{\alpha\beta}(z-\zeta)E_\beta(\zeta)d\zeta \tag{13}$$

where

$$K_{\alpha\beta}(x) = -\frac{2e^2}{(2\pi\hbar)^3}\int_{v_z>0}\frac{v_\alpha v_\beta}{v_z}\cdot\frac{\partial w_0}{\partial\varepsilon_e}\exp\left(-\frac{|x|}{v_z\tau_1}\right)d^3p.$$

We now calculate the Fourier image of the kernel $K_{\alpha\beta}(x)$

$$\begin{aligned}\tilde{K}_{\alpha\beta}(\kappa) &= \int_{-\infty}^{\infty} K_{\alpha\beta}(x)\exp(-i\kappa x)dx \\ &= -\frac{4e^2}{(2\pi\hbar)^3}\int_{v_z>0}\frac{\tau_1 v_\alpha v_\beta}{1+\kappa^2 v_z^2\tau_1^2}\frac{\partial w_0}{\partial\varepsilon_e}d^3p. \end{aligned}\tag{14}$$

To calculate the integral over the momentum space, we make use of the spherical Fermi surface approximation and neglect the temperature smearing of the Fermi distribution, $((\partial w_0)/(\partial\varepsilon_e)) \cong -\delta(\varepsilon_e - \varepsilon_F)$, where $\varepsilon_F = p_F^2/2m$ is the Fermi energy, p_F is the Fermi momentum, $\delta(\varepsilon_e - \varepsilon_F)$ is the Dirac delta function, and m is the effective mass of electrons. Upon integration over the angles, we obtain

$$\tilde{K}_{\alpha\beta}(\kappa) = \delta_{\alpha\beta}\cdot\frac{4\pi e^2 p_F^2}{(2\pi\hbar)^3\kappa}g(\kappa\cdot v_F\tau_1) \tag{15}$$

where $\beta = x, y$, $\delta_{\alpha\beta}$ is the Kronecker delta, $v_F = p_F/m$, and $g(x) = \mathrm{arctg}(x) + ((\mathrm{arctg}(x) - x)/(x^2))$.

For the field $\vec{E}$ in a metal, according to (7) and (13), we have

$$\frac{d^2E_\alpha}{dz^2} = -\frac{4\pi\omega\cdot i}{c^2}\int_{-\infty}^{\infty}K_{\alpha\beta}(z-\zeta)E_\beta(\zeta)d\zeta. \tag{16}$$

At the boundary of the metal, the derivative $((dE_\alpha)/dz)$ undergoes a jump, since the electric field was considered as continued symmetrically to the region $z < 0$. With this in mind, the equation for the field takes the form

$$\frac{d^2E_\alpha}{dz^2} - 2E'_\alpha(0)\cdot\delta(z) = -\frac{4\pi\omega\cdot i}{c^2}\int_{-\infty}^{\infty}K_{\alpha\beta}(z-\zeta)E_\beta(\zeta)d\zeta. \tag{17}$$

We now perform the Fourier transform for both sides of the equation and take into account the diagonality of $K_{\alpha\beta}$

$$-\kappa^2\tilde{E}_\alpha - 2E'_\alpha(0) = -\frac{4\pi\omega\cdot i}{c^2}\tilde{K}_{\alpha\alpha}\tilde{E}_\alpha. \tag{18}$$

This results in the following expression for the surface impedance ζ:

$$\begin{aligned}\xi &= \left.\frac{E_x}{H_y}\right|_{z=0} \\ &= \frac{\omega\cdot i}{c}\cdot\frac{E_x}{E'_x(0)} \\ &= \left\{\frac{\omega\cdot i}{c}\cdot\frac{1}{2\pi}\cdot\int_{-\infty}^{\infty}\frac{2\exp(i\kappa z)}{\frac{4\pi\omega\cdot i}{c^2}\tilde{K}_{xx}-\kappa^2}dk\right\}_{z=0}. \end{aligned}\tag{19}$$

We obtain the following expression for ξ by using (15) and (19) and performing some transformations:

$$\xi = \left(\frac{4k_0^2}{\pi^2\alpha k_F^2}\right)^{1/3}\cdot\int_0^\infty\frac{u}{g(\beta u)+iu^3}du \tag{20}$$

where $\alpha = ((e^2)/(\hbar c))$ is the constant of the fine structure, $k_F = ((p_F)/\hbar)$, and $\beta = ((v_F\tau)/(1-i\omega\tau))(((2\alpha)/\pi)k_0k_F^2)^{1/3}$.

Expression (20) makes it possible to analyze the main features of the dependence of the surface impedance on the frequency and electron's mean free path time. Consider the following three limiting cases.

1)
$$\begin{cases}\tau \ll \dfrac{1}{v_F}\cdot\left(\dfrac{2\alpha}{\pi}k_0k_F^2\right)^{-1/3} \\ \tau \ll \dfrac{1}{\omega}\end{cases}$$
then
$$g(\beta u) \cong u\cdot\left(\frac{2}{3}v_F\tau\left(\frac{2\alpha}{\pi}k_0k_F^2\right)^{1/3}\right)$$
can be put under integral (20), and the integral will be taken as $\xi = (\omega/(8\pi\sigma))^{1/2}(1-i)$, which coincides with the surface impedance in the case of the normal skin effect.

2)
$$\begin{cases}\tau \gg \dfrac{1}{v_F}\cdot\left(\dfrac{2\alpha}{\pi}k_0k_F^2\right)^{-1/3} \\ \omega \ll v_F\cdot\left(\dfrac{2\alpha}{\pi}k_0k_F^2\right)^{1/3}\end{cases}$$

(the second condition approximately corresponds to $f \ll 10$ THz), then $g(\beta u) \cong \pi/2$, and the surface impedance becomes independent of τ, which corresponds to the extremely anomalous skin effect, $\xi = (2/3)((k_0^2)/(\alpha k_F^2))^{1/3} \cdot ((\sqrt{3}/3) - i)$.

3)

$$\begin{cases} \tau \gg \dfrac{1}{\omega} \\ \omega \gg v_F \cdot \left(\dfrac{2\alpha}{\pi} k_0 k_F^2\right)^{1/3} \end{cases}$$

then

$$g(\beta u) \cong \frac{2i}{3}\frac{v_F}{\omega}\left(\frac{2\alpha}{\pi}k_0 k_F^2\right)^{1/3} \cdot u$$

which corresponds to the so-called relaxation region. In this case, the surface impedance is a purely imaginary quantity, and the reflectance is therefore equal to unity, $\xi = -i((2)/(3))^{1/2}(\omega/(\omega_p))$, where $\omega_p = 4\pi e^2 n/m$ is the plasma frequency; here, $n = k_F^3/3\pi^2$ is the electron density.

To study the dependence of the surface impedance on temperature, it is needed to know the form of the dependence $\tau(T)$. The mean free path time is related to the d.c. conductance by

$$\tau = \frac{m\sigma}{ne^2}. \tag{21}$$

For pure metals, an approximate formula of the dependence $\sigma(T)$, which is in good agreement with the experiment, is well known [15]

$$\sigma_0(T) = C \cdot \left(\frac{\theta}{T}\right)^5 \left(\int_0^{\theta/T} \frac{x^5}{\mathrm{ch}(x) - 1}\right)^{-1} \tag{22}$$

where C is a constant, which is determined experimentally, and θ is the Debye temperature of the metal. The presence of a small amount of impurities leads to a residual resistance, so another formula is valid for the conductivity

$$\sigma(T) = \tilde{C} \cdot \left(\left(\frac{T}{\theta}\right)^5 \cdot \int_0^{\theta/T} \frac{x^5}{\mathrm{ch}(x) - 1} + \gamma \frac{N_c}{N}\right)^{-1} \tag{23}$$

where N_c/N is the ratio of the number of impurity atoms to the total number of atoms (it is assumed that $N_c \ll N$), γ is a constant coefficient, which depends on the sort of impurities and the properties of the metal. In general, $\tilde{C} \neq C$, but for many impurities, these coefficients can be assumed equal. Expression (23) can be written in another form

$$\sigma(T) = (A/\sigma_0(T) + \rho_0)^{-1} \tag{24}$$

where ρ_0 is the residual resistance and A is a dimensionless coefficient.

Thus, the temperature dependence of the reflectivity of real metal samples in the millimeter and submillimeter ranges can be approximately described using (8), (20), (21), and (24). It should be noted that this dependence does not allow for many factors that can significantly affect the reflectivity, for example, the presence of the surface structure of the sample, nonsphericity of the Fermi surface, a more complex form of the boundary condition for electrons on the metal surface, a more complex nature of the influence of impurities on the metal conductivity, etc. A comparison of the experimental data with such a simplified model is given in Section IV.

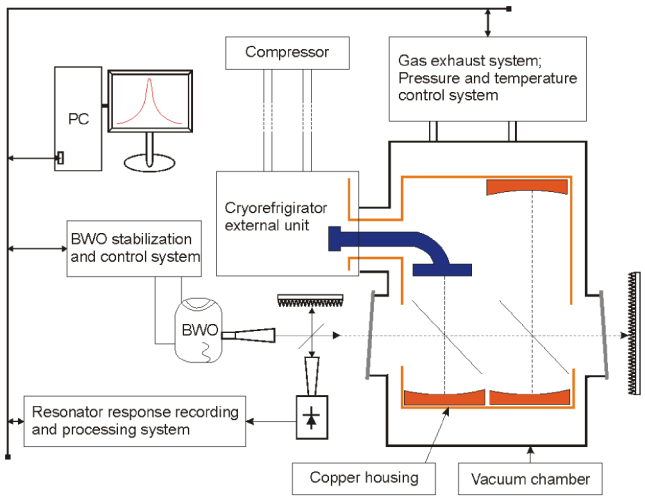

Fig. 2. Block diagram of the experimental setup.

III. Experimental Setup and Measurement Procedure

The experimental setup described in [8] was created on the basis of a resonator spectrometer with a precision frequency stabilization system of the millimeter and submillimeter radiation sources [16]. A block diagram of the experimental setup is shown in Fig. 2. The excitation, recording, and processing system of the resonator signal is described in detail in [16] and [17].

To date, the spectrometer can be operated in the frequency band 45–520 GHz, which is divided into several subbands determined by the characteristics of the radiation sources [backward-wave oscillators (BWOs)]. Subband switching takes a few minutes and is performed by replacing the unit, which includes a BWO and related waveguide–quasi-optical line. In the most high-frequency subband 350–520 GHz, a cooled InSb bolometer is used as the receiver of radiation [18] and Schottky-barrier diodes are used for the lower frequencies.

Two quasi-optical Fabry–Perot resonators of twice as different length located in the vacuum chamber are used as the sensitive elements of the setup. The longer resonator is formed by two identical spherical mirrors and the shorter resonator is formed by one spherical mirror and one flat mirror, which is the test sample. Three spherical mirrors are identical and were manufactured using the same technology. Identical dielectric films of Teflon with 4-μm thickness are arranged at an angle of 45° and placed in the resonators as the coupling elements. The test samples are metal disks about 50 mm in diameter, with the surface treated by a diamond cutter with a surface roughness of 10–20 nm. To examine the reflectivity of silver and gold, the corresponding metals were deposited on a copper mirror in vacuum or using a galvanic technique so as to obtain a 1-μm-thick layer.

The principle of measuring the reflection loss of a metal sample is based on determining the Q-factor of the Fabry–Perot resonator, which depends on the energy loss inside the resonator. In the case where the resonator is in vacuum (or in a nonabsorbing gas), the following formula can be used for the loss calculation:

$$D_{\text{tot}} = D_{\text{refl}} + D_{\text{coupl}} + D_{\text{difr}} = \frac{2\pi L \Delta f}{c} \tag{25}$$

where D_{tot} is the total loss (dissipation) of energy in one traversal of the resonator, D_{refl} is the energy dissipation in the mirrors, D_{coupl} is the coupling loss, D_{difr} is the diffraction loss, and L is the resonator length. By choosing the corresponding geometric parameters of the resonator (length, curvature radius, and diameter of the mirrors), we make the diffraction loss negligibly small compared with the other terms. Thus, writing (25) for the longer and shorter resonators, we obtain

$$\begin{aligned} \frac{1}{2}(D_{\text{smpl}} + D_{\text{mirr}}) + D_{\text{coupl}} &= \frac{2\pi L_1 \Delta f_1}{c} \\ D_{\text{mirr}} + D_{\text{coupl}} &= \frac{4\pi L_1 \Delta f_2}{c} \end{aligned} \tag{26}$$

where $D_{\text{smpl}} = 1 - R_{\text{smpl}}$ is the energy loss due to reflection from the sample, D_{mirr} is the energy loss due to reflection from spherical mirrors, Δf_1 and Δf_2 are the widths of the resonance curves of the shorter and longer resonators, respectively, and L_1 is the length of the shorter resonator. From (26), we obtain an expression for the sample reflectance

$$1 - R_{\text{smpl}} = \frac{4\pi L_1}{c}(\Delta f_1 - \Delta f_2) - D_{\text{coupl}}. \tag{27}$$

Equation (27) contains four quantities on the right-hand side, namely, L_1, Δf_1, Δf_2, and D_{coupl}, which are determined with high accuracy by measuring the resonator resonance frequencies. The resonator length L_1 is determined by measuring the frequency-scale distance δf between two successive longitudinal resonator modes using the formula

$$L_1 = \frac{c}{2\delta f}. \tag{28}$$

The error of determining the resonator length by such a method is less than 1 μm (the shorter resonator being about 350 mm long). The width of the resonance curve is determined by numerically fitting the Lorentzian profile (with added linear and constant terms) to the digital record of the resonator response [16]. To increase the accuracy of determining the width of the resonance curve, 128 direct and inverse scans are performed. As a result, a statistical error of determining the resonance curve width of about 50 Hz for its value of about 100 kHz is achieved.

The loss introduced by the coupling film is determined by the transmission coefficient of the dielectric film, which depends on its thickness, as well as the real and imaginary parts of the dielectric permittivity. This loss is measured in a separate experiment. To do this, besides one coupling film, another film, for which the energy dissipation should be measured, is placed additionally in the Fabry–Perot resonator. The additional loss introduced by the second film is determined by the formula

$$D_{\text{coupl}} = \frac{2\pi L}{c}(\Delta f_{2\text{film}} - \Delta f_{1\text{film}}) \tag{29}$$

where $\Delta f_{2\text{film}}$ and $\Delta f_{1\text{film}}$ are the widths of the resonance curve in a resonator with two and one films, respectively. In principle, it is possible to omit the latter term on the right-hand side of (27) if two identical dielectric films are placed at once in the longer resonator, as was done in the earlier experiments [19]. In this paper, such an approach is not used since it involves technical difficulties, and it is much easier to measure the loss introduced by the coupling film in a separate experiment.

Thus, all the quantities in (27) for determining the reflectance of the studied sample are found from frequency measurements with low error and good repeatability. The resonance method of measurement is also most sensitive; as a result, the minimum measurable reflection loss (D_{smpl}) is less than 10^{-4}.

The statistical error of determining the reflection loss from (27) is on the order of 0.1%. However, the real error of the obtained results is higher due to the standing wave effect in the quasi-optical line of the experimental setup. The frequency dependence of the width of the resonance curve appears to be modulated with an amplitude of about 10% due to the interference of the resonance response signal with spurious reflections mainly from the detector. This modulation is irregular and differs for the longer and the shorter resonators, which impedes its exact account. Correspondingly, in the measurement at one fixed frequency point we have an additional error of about 10% due to this effect. The problem can be solved by averaging the obtained result at several frequency points. The reflection loss of pure metals is characterized by a smooth power-law dependence on frequency (the exponent is 0.5 near the room temperature and 0.67 in the anomalous skin-effect limit). When the dependence is averaged, for example, at six frequency points in the range 200–250 GHz, a reflection loss error of about 5% is reached, which is sufficient both for most applications and for a theoretical analysis of the results.

The resonators were placed in a stainless-steel vacuum chamber isolated from the environment. Input and output windows made of high-pressure polyethylene were arranged at an angle of 10° (Fig. 2) to prevent penetration of the reflected radiation to the detector. The vacuum chamber is equipped with a gas inlet and pumping system, which includes foreline and high-vacuum pumps and pressure sensors. For cooling of the sample we used a closed-cycle cryogenic refrigerator with a Gifford–McMahon thermodynamic cycle of the helium temperature level, which is capable of cooling to a temperature of less than 3 K at the second stage and to 60 K at the first stage without any load. The first stage of the refrigerator is connected to a 5-mm-thick copper housing, isolated from the walls of the vacuum chamber and with the resonators located inside. The temperature gradient in the housing does not exceed 2° when it is cooled to 70 K. The second stage is connected to the test sample (a flat mirror of the shorter resonator) through a flexible copper cold finger.

A photograph of the experimental setup is shown in Fig. 3(a). The instrumental rack including a BWO power supply, a frequency synthesizer, and a PC is located on the left of the photograph. The BWO connected to the waveguide–quasi-optical line and the vacuum chamber with the resonators

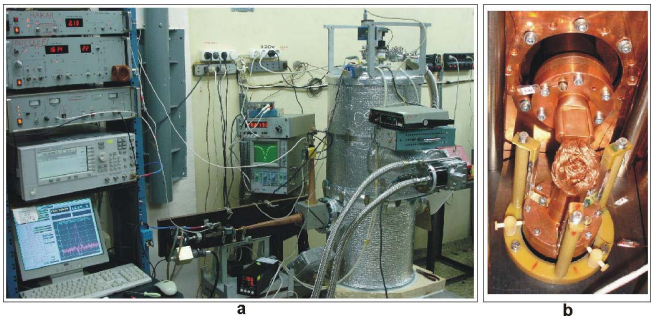

Fig. 3. (a) Photograph of the experimental setup. (b) Photograph of the test sample (a flat mirror of the shorter resonator), which is connected to the second stage of the refrigerator through a flexible copper cold finger.

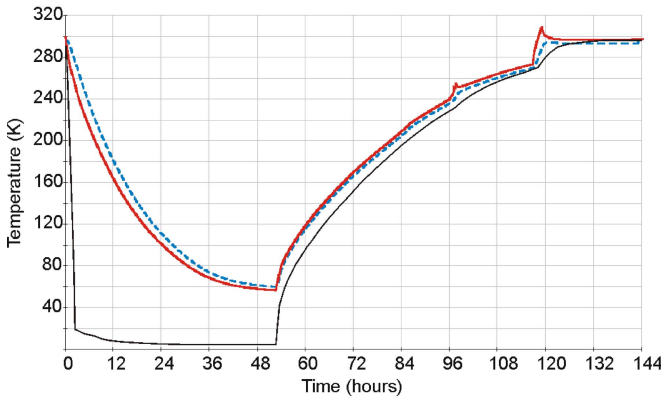

Fig. 4. Temperature dependence on the time in the experiment. Black thin solid line: temperature of the sample (flat mirror). Red thick solid line: temperature of the copper housing. Blue thick dashed line: average temperature of the spherical mirrors.

are located in the middle lower and the right parts of the photograph, respectively. Fig. 3(b) demonstrates a photograph of the test sample, which is connected to the second stage of the refrigerator.

The chamber is evacuated before cooling. The temperature of the mirrors, the housing, and the sample is controlled by an eight-channel automated system with Lake Shore DT-670B-CU diode thermal sensors with a nominal accuracy of ± 0.5 K in the range 2–305 K. Fig. 4 shows a diagram of temperature variation in the experiment. It is seen in the figure that the sample temperature decreases rapidly to 20 K and then slowly, for approximately 48 h, to 4 K, while the temperature of the copper housing and spherical mirrors reaches approximately 60 K.

The temperature dependence of the resonance curve widths is performed during natural heating. Once the sample reached a temperature exceeding 200 K, a short-term additional heating of the housing was also switched on to speed up the sample heating (spikes on the curve in Fig. 4).

IV. Results

A. Copper

We have studied two different samples of copper. One of them is made of classical oxygen-free (OF) copper (99.97% Cu) and the other, of highly pure (99.999% Cu) monocrystalline OF copper produced by

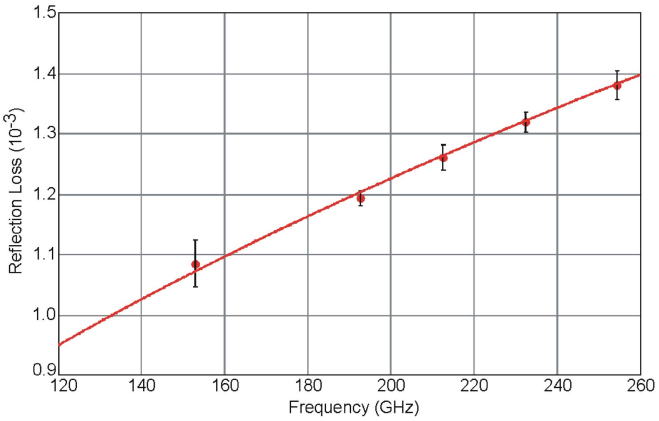

Fig. 5. Reflection loss for a mirror of HP copper at $T = 295$ K versus frequency. The points correspond to the experiment data, the vertical lines show their error, and the solid line is approximation by the root dependence.

SIBNEOTEK Ltd. (hereafter referred to as HP copper). It should be mentioned that here and henceforth we use manufacturer's data on chemical composition of materials (from quality certificates or test results). For example, for the HP copper sample the total impurities evaluation was made by spark source mass spectrometry.

The studied samples were first measured at room temperature. The obtained data on their reflectivity were compared with the reference data for pure metals in accordance with the normal skin-effect theory. As the example, frequency dependence of the reflection loss of a sample of HP copper at $T = 295$ K is shown in Fig. 5. The resulting experimental points are approximated by a dependence of the form $1 - R_{\mathrm{Cu}} = 8.67(2) \times 10^{-5} \cdot f^{0.5}$, where f is the frequency in gigahertz. Hence, using (3), we find that $\sigma_{\mathrm{Cu1}} = 5.32(2) \cdot 10^{17}$ s^{-1} (reference data [20], [21]: $\sigma_{\mathrm{Cu}}(295\ \mathrm{K}) = 5.31 \times 10^{17}$ s^{-1}). The conductivity in CGS units can be expressed over the resistivity in SI units as follows: $\sigma\ [\mathrm{s}^{-1}] = 9 \times 10^9/\rho\ [\Omega\mathrm{m}]$. Although usually the reference books give data on the conductivity of polycrystalline copper, and the studied sample was made of monocrystalline copper, there is coincidence between the experimental data and the reference results within the error of measurements. For OF copper, the loss was higher and the conductivity was lower, namely, $\sigma_{\mathrm{Cu2}} = 4.28(14) \cdot \times 10^{17}$ s^{-1}, which can be explained by the influence of impurities.

The sample of OF copper was measured at cryogenic temperatures only at a frequency of 150 GHz, and the sample of HP copper was measured at seven frequency points in the range 190–250 GHz. In addition, the measurements were repeated several times for the HP copper sample to increase the reliability of the results and delete some nonphysical "spikes" in the reflection loss versus temperature dependence. Such spikes, which can possibly be explained by the mechanical strain in the sample mounting construction, vanish after several cooling-heating cycles. Another series of measurements was performed after the sample was annealed at $T = 800$ °C in the hydrogen atmosphere.

Fig. 6 shows the reflection loss versus temperature for OF copper at a frequency of 150 GHz. The sample loss at

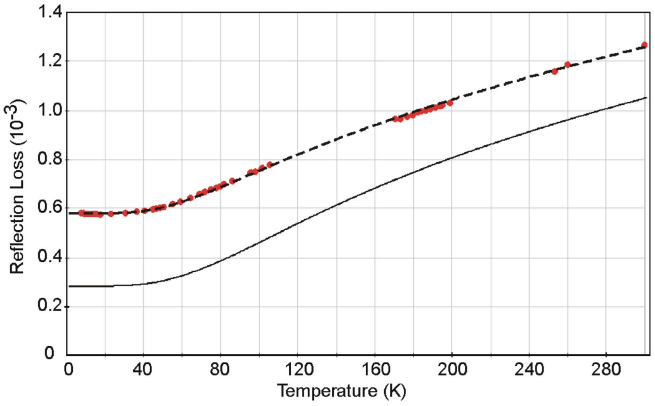

Fig. 6. Reflection loss for copper at a frequency of 150 GHz versus temperature. The thin solid line is a calculation for pure copper having regard to the anomalous skin effect. Dots: experimental dependence for the OF copper sample. Thick dashed line: approximation of this dependence by the model using (20), (21), and (24). Hereafter, the relative error of determining the reflection loss is about 10% if the measurements are performed at one frequency and about 5% in the case of averaging over the frequency range.

$T < 40$ K is about two times higher than the calculated value. To approximate the observed experimental dependence, we calculated power reflectance using (8) and (20). The mean free path time τ was expressed through conductivity $\sigma(T)$ from (21). Equations (22) and (24) were used to simulate the conductivity versus temperature dependence. For the best description of the observed dependence, the following parameters in (24) were chosen: $A = 1.09$ and $\rho_0 = 0.56 \times 10^{-8}\ \Omega \cdot$ m. It should be mentioned that within the framework of this model, the anomalous skin effect is fully absent since the condition $v_F \tau \gg (2\alpha k_0 k_F^2/\pi)^{-1/3}$ is not fulfilled even at the lowest temperatures. The observed "saturation" in the temperature dependence below 40 K indicates that the residual resistance is reached.

For direct comparison of these results with those obtained at other frequencies, it is needed to know the dependence of the loss on frequencies over the entire range of temperatures. For OF copper, this dependence was not studied experimentally, but it can be obtained from theoretical considerations. To do this, we used (8), (20), (21), and (24) in which the above-mentioned parameters A and ρ_0 were substituted. The calculated dependence of the reflection loss $D(f)$ in the frequency range 5–260 GHz at fixed values of the temperature from 4 to 300 K with 10 K step was modeled by a dependence of the form $K \cdot (f/f_0)^{nf}$. Fig. 7 shows the parameter n_f as a function of temperature. A similar dependence obtained for the parameters $A = 1.0$ and $\rho_0 = 0$, i.e., for pure copper, and the dependence for HP copper in the frequency range 190–250 GHz, which was determined from the experiment, are also shown in Fig. 7. The latter dependence was determined by fitting the above-mentioned power function to the experimental points corresponding to one value of temperature and different frequencies. Comparing the obtained dependences, it is seen that in the experiment with annealed HP copper, the parameter n_f tends to decrease with increasing temperature, similar to the calculated dependence, but its absolute value at cryogenic temperatures is, on the average, higher than the calculated one.

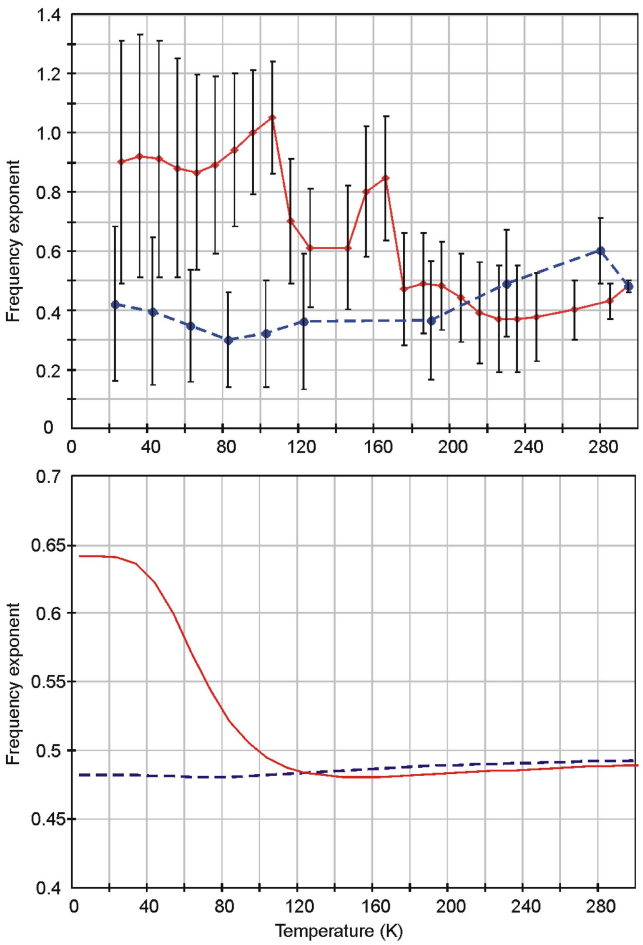

Fig. 7. Temperature dependence of the exponent of the frequency dependence of the reflection loss for copper. Bottom: red solid line is a calculation for pure copper and the blue dashed line is a calculation for copper with residual resistance (see the text). Top: experimental dependences obtained in the range 190–250 GHz for HP copper (blue dashed and red solid lines correspond to the samples before and after the hydrogen annealing, respectively). The vertical lines show the standard deviation ($\pm 1\sigma$).

The large error of determining this parameter does not permit any precise conclusions on the character of the dependence obtained in the experiment. As for nonannealed copper, the dependence of the parameter n_f on temperature is virtually absent, which is closer to the calculations for copper with residual resistance.

The initial data processing by the method described above was used to convert all the temperature dependences to one frequency $f = 230$ GHz. Fig. 8 shows the corresponding temperature dependences, their approximation, and a calculation for pure copper.

The HP copper sample after the hydrogen annealing demonstrates the least loss at cryogenic temperatures, which exceeds the calculated loss by about 25% (before the annealing, the difference was about 45%). The annealing did not affect the loss value at room temperature. We can assume that the observed effect is due to changes in the structure of the surface layer of copper as a result of annealing. The OF copper sample has a higher loss at room temperature, and especially at cryogenic temperatures (the difference from the calculation for pure copper is almost twofold).

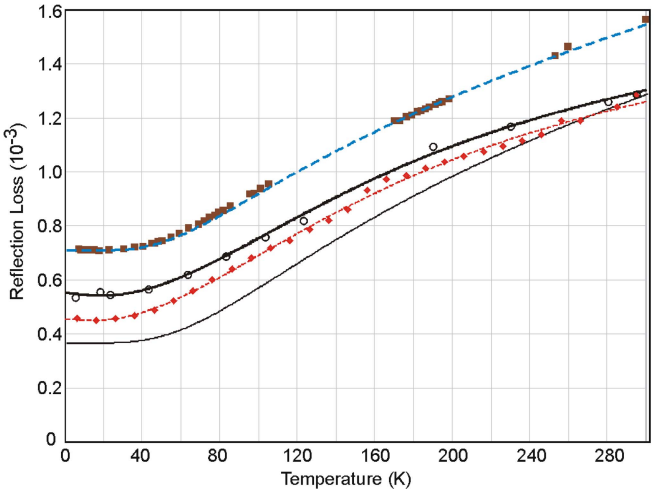

Fig. 8. Reflection loss for copper samples at a frequency of 230 GHz versus temperature. Black thin solid line: calculation for pure copper having regard to the anomalous skin effect. Squares: conversion of the experimental dependence obtained for a sample of OF copper at a frequency of 150 GHz (see the text). Blue thick dashed line: approximation of this dependence by the model using (20), (21), and (24). Circles: experimental dependence for a sample of HP copper (averaged over several frequencies in the range 190–250 GHz). Black thick solid line: approximation of this dependence (see the text). Diamonds: experimental dependence for a sample of HP copper after the hydrogen annealing (averaged over several frequencies in the range 190–250 GHz). Red thin dashed line: approximation of this dependence (see the text).

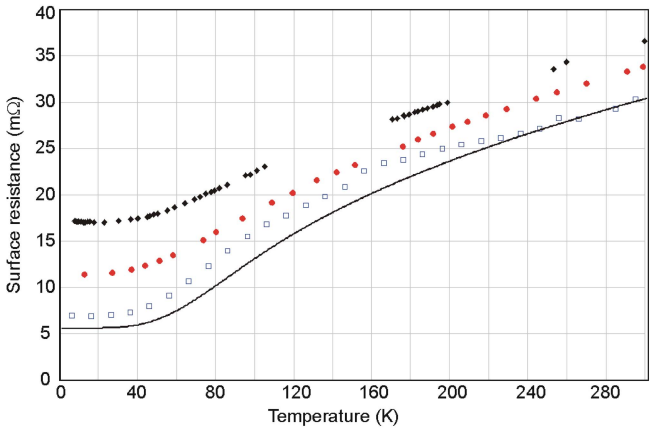

Fig. 9. Surface resistance of copper (mΩ) at a frequency of 13.6 GHz versus temperature. Black solid line: calculation for pure copper having regard to the anomalous skin effect. Diamonds: conversion of the experimental dependence obtained for the sample of OF copper at a frequency of 150 GHz. Circles: experimental data for OF copper from [23]. Squares: conversion of the experimental dependence obtained for the sample of HP copper after the hydrogen annealing in the frequency range 190–250 GHz.

It should be mentioned that the character of the experimental dependence $D(T)$ for the sample of HP copper and for most of other samples (except for OF copper and aluminum) cannot be described satisfactorily in terms of the model based on the use of (20), (21), and (24). Therefore, to approximate the experimental points by a continuous curve, we chose an empirical dependence which correctly describes the observed points

$$D(T) = \eta \exp(-\lambda T) \cdot T^{nt} + \gamma\,(1 - \exp(-\lambda T)) \cdot \sqrt{T} + \mu \tag{30}$$

where the parameter nt was fixed for all the observed dependences corresponding to the given metal (for copper, it is equal to 1.5) and the parameters η, λ, γ, and μ are determined by fitting the model to the experimental dependence using the least squares method. A drawback of such an empirical model is that most of its parameters have no physical meaning [the parameter γ can be assumed as a coefficient of proportionality between the loss value and the root from the temperature at high temperatures where $\sigma \sim 1/T$, see (3)]. However, this model describes well all the dependences observed in the experiment.

It is interesting to compare our data with the previous results. Analysis of publications on the subject shows that the measurement of the reflection loss of pure metals at the frequencies $f \geq 150$ GHz when cooled down to 4 K was first performed in [8].

There are earlier works devoted to the study of the surface impedance of materials at cryogenic temperatures in the microwave range [22], [23] using waveguide equipment and resonant chambers. Such measuring techniques are effective at frequencies not exceeding ~40 GHz. Despite this, our data can be compared with other works by converting them to the lower frequency region. In particular, a temperature dependence of the surface resistivity (a quantity proportional to the real part of the surface impedance) of OF copper in the range 14–300 K at a frequency of 13.6 GHz was obtained in [23]. The reflection loss $D(T)$ was converted for OF copper (Fig. 6) to the frequency 13.6 GHz, and then the surface impedance was calculated via the reflection loss using the formula

$$R_s[\Omega] = \frac{2\pi \cdot 3 \cdot 10^{10}}{0.5 \cdot 4 \cdot 10^{9}} \cdot D \tag{31}$$

which was obtained from the ratio of impedances in the SI and CGS systems. The result of comparison is presented in Fig. 9. The surface impedance of copper measured in [23] over the entire frequency range is lower than the result of conversion of our data for OF copper, but higher than the result of a similar conversion for HP copper. This result is understandable since there are several sorts of OF copper which differ in the chemical composition of impurities, leading to a difference in the observed surface resistance. In this regard, it is of interest to measure the same sample (HP copper) in different frequency ranges.

B. Aluminium

The temperature dependence of the reflection loss for mirrors of highly pure aluminum (99.99% Al) was determined for one frequency $f = 150$ GHz. The corresponding dependence is shown in Fig. 10. The reflection loss for this sample at cryogenic temperatures exceeds the calculated value by about 65%.

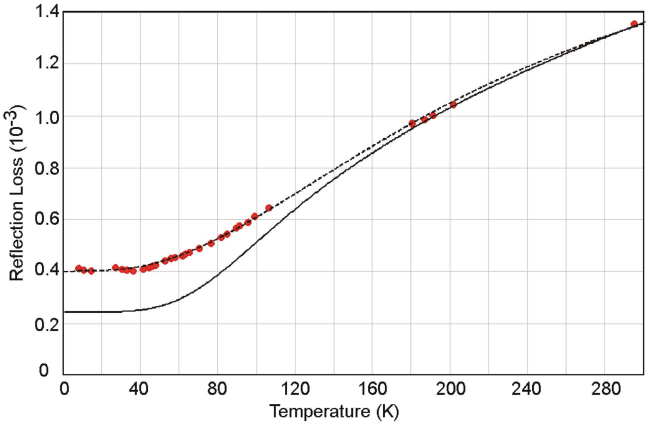

Fig. 10. Reflection loss of aluminum at a frequency of 150 GHz versus temperature. Solid line: calculation for pure aluminum having regard to the anomalous skin effect. Points: experimental dependence for HP aluminum. Dashed line: approximation of this dependence by an empirical model using (30).

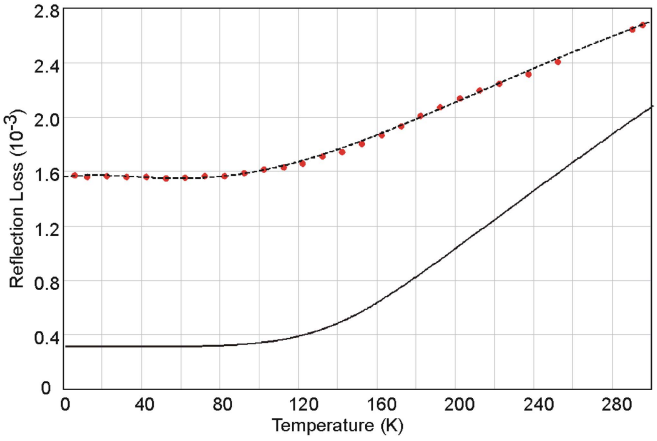

Fig. 11. Reflection loss of beryllium at a frequency of 230 GHz versus temperature. Solid line: calculation for pure beryllium having regard to the anomalous skin effect. Points: experimental dependence for the sample of 97.8% beryllium (averaged over several frequencies in the range 200–250 GHz). Dashed line: approximation of this dependence by an empirical model using (30).

C. Beryllium

We have studied a sample made of a technical alloy with beryllium content 97.8%. This material, unlike pure beryllium, is constructional, and from this material it is planned to manufacture a cooled switching mirror of the Millimetron space observatory [24]. In this regard, the task was given to determine the reflection properties of the material as it is cooled down to 4 K. Furthermore, the study of the reflectivity of beryllium is interesting for the reason that this metal has a high Debye temperature $\theta = 1481$ K, resulting in that its resistance decreases abruptly with decreasing temperature, as follows from (22). It follows from calculations that even at $T = 100$ K the reflection loss for beryllium almost reaches the limiting low value, while for the other metals (Al, Au, and Cu), this occurs only below 40 K.

Because of the relatively high content of impurities, the reflectivity of the sample was significantly worse than it follows from the calculation for pure beryllium, as is demonstrated in Fig. 11. Based on the above studies, it was proposed to cover the switching mirror with gold as the most stable and reproducible reflective material.

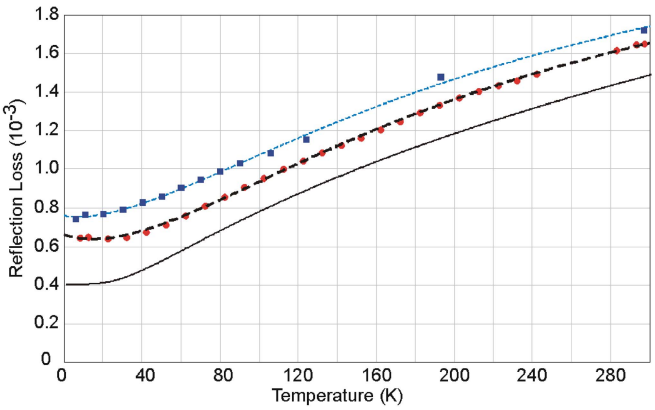

Fig. 12. Reflection loss of gold at a frequency of 230 GHz versus temperature. Black thin solid line: calculation for pure gold having regard to the anomalous skin effect. Circles: experimental dependence for the sample with galvanically deposited gold (averaged over several frequencies in the range 200–250 GHz). Black thick dashed line: approximation of this dependence by an empirical model using (30). Squares: experimental dependence for the sample of vacuum deposited gold (averaged over several frequencies in the range 200–250 GHz). Blue thin dashed line: approximation of this dependence by an empirical model using (30).

D. Gold

Gold is a chemically resistant metal characterized by a high conductivity, which is inferior in this parameter only to silver and copper. This causes extensive use of the gold coating of materials, including reflectors. In this paper, we have studied two samples with gold coating, namely, galvanic coating and a vacuum deposition coating by 99.99% gold. The coating was deposited on a copper mirror. The thickness of the gold layer was no less than 1 μm, which is several times greater than the depth of the skin layer in this frequency range. The measurement results are shown in Fig. 12.

It is interesting to note that the galvanic gold coating has a smaller loss than vacuum deposited gold, although the latter should be chemically purer. Probably, the reason for such a difference is the different structure of the reflecting surface.

Another interesting result obtained for galvanic gold is a detailed temperature dependence of the exponent n_f of the frequency dependence (Fig. 13). This dependence is different from the calculation performed using (20)–(22), but it coincides with calculations near $T = 4$ K and $T = 300$ K.

E. Silver

Silver, as well as gold, is also widely used for the mirror coating. In particular, the quasi-optical resonator mirrors used in our experimental setup are coated with a layer of vacuum-deposited silver over which a protective layer of aluminum oxide is applied. The sample obtained by a similar technology from 99.99% silver has been examined. The results are presented in Fig. 14.

The observed significant excess of the loss in the silver-coated mirrors compared with the theoretically calculated dependence most likely indicates a significant influence of the surface structure on the reflectance. The silver-coated spherical mirrors have a little worse reflectivity in comparison to the

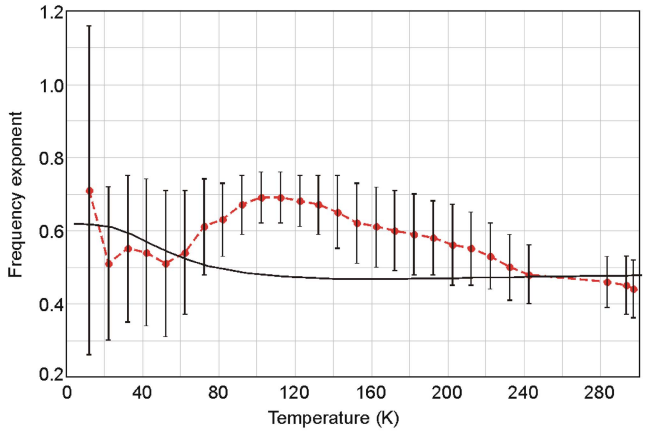

Fig. 13. Exponent of the frequency dependence of gold reflection loss versus temperature. Black solid line: calculation for pure gold. Red dashed line: experimental dependence obtained in the range 200–250 GHz for galvanic gold. Vertical lines: standard deviation ($\pm 1\sigma$).

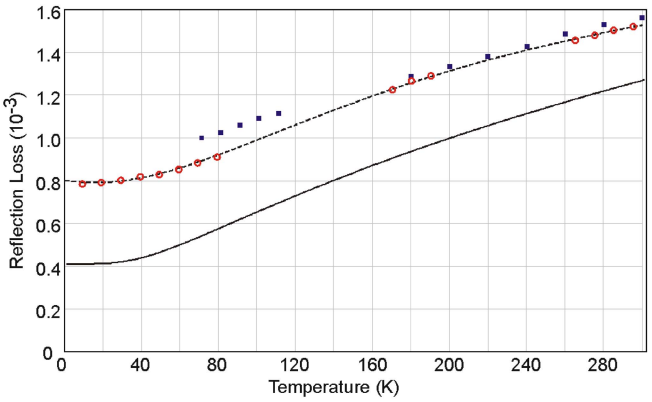

Fig. 14. Reflection loss of silver at a frequency of 230 GHz versus temperature. Solid line: calculation for pure silver having regard to the anomalous skin effect. Circles: experimental dependence for the sample of vacuum deposited silver (averaged over several frequencies in the range 200–250 GHz). Dashed line: approximation of this dependence by an empirical model using (30). Squares: experimental dependence for our spherical mirror coated with a layer of silver and a protective coating of aluminum oxide.

studied sample, especially at $T < 120$ K, which can be caused by the effect of the environment (the resonators with these mirrors have been used for several years, including the investigation of absorption in heated water vapor). This experiment permits one to estimate the possibility of increasing the sensitivity of the resonator spectrometer by cooling the resonator mirrors. If the silver mirrors made by the vacuum deposition technology are used, then the maximum achievable gain in sensitivity will not exceed two times (Fig. 14). If high-purity copper mirrors are used, then the loss can be reduced by almost another two times by cooling the mirrors to below 40 K. However, such a method of increasing the sensitivity is technically difficult, and the possibility of its application is limited. Cold mirrors are difficult to isolate from the warm medium under study (gas).

V. Contribution to the Noise Temperature of Antenna Reflectors

One of the practical problems solved within the framework of this paper is estimation of the effect of the thermal

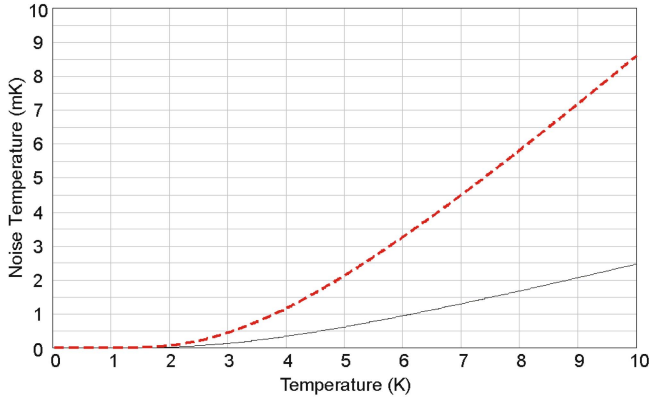

Fig. 15. Noise temperature of mirrors versus their physical temperature, which is calculated on the basis of the experimental data on reflection loss. Black thin solid curve: calculation for the HP copper sample after the hydrogen annealing. Red thick dashed line: calculation for the mirror made of a technical beryllium alloy.

radiation from the reflectors of the Millimetron space mission on highly sensitive receivers. To do this, we calculated the brightness temperature of the cooled mirrors. According to the Rayleigh–Jeans distribution, the relationship between the radiation intensity of an absolutely black body radiation and its temperature is expressed by

$$I = k_b T \cdot \frac{2f^2}{c^2} \tag{32}$$

where k_b is the Boltzmann constant. This expression is valid until $\hbar\omega \ll k_b T$. At the lower temperatures, this approximation is no longer valid, but the temperature determined by (32) can still be used as a power unit, namely, the brightness temperature $T_{\rm br}$, which characterizes the radiation intensity. The intensity itself is determined by the Planck formula

$$I = \frac{2f^2}{c^2} \cdot \frac{\hbar\omega}{\exp(\hbar\omega/k_b T) - 1}. \tag{33}$$

We can determine the brightness temperature of an absolutely black body via its physical temperature using (32) and (33)

$$T_{\rm br} = \frac{\hbar\omega/k_b T}{\exp(\hbar\omega/k_b T) - 1} \cdot T. \tag{34}$$

For the metal having a power reflectance R, we obtain

$$\begin{aligned} T_{\rm br} &= (1 - R) \cdot \frac{\hbar\omega/k_b T}{\exp(\hbar\omega/k_b T) - 1} \cdot T \\ &= D \cdot \frac{\hbar\omega/k_b T}{\exp(\hbar\omega/k_b T) - 1} \cdot T. \end{aligned} \tag{35}$$

It is possible to calculate the brightness (noise) temperature of a mirror versus its physical temperature using (35) and the dependence $D(T)$ determined from the experiment. Fig. 15 shows such a dependence at a frequency of 230 GHz for HP copper sample (after the hydrogen annealing) and a sample made of a technical alloy of beryllium (these samples are characterized by the minimum and maximum losses, respectively, among all the studied samples).

At a temperature of 4 K, the best sample is characterized by a noise temperature of less than 0.5 mK, and the worst, a little more than 1 mK. Although these quantities are extremely small compared with the noise temperatures of the receivers,

they are by far superior, for example, to the anisotropy of the relic radiation ($\sim 10^{-5}$ K), which is observed in modern observatories with supersensitive receivers [4]. It should be borne in mind that the thermal radiation comes to the receiver from several mirrors of the receiving system, and the power of the noise sources is summarized.

VI. Conclusion

In this paper, a detailed experimental study of the reflectivity of metals in the millimeter wavelength range at a temperature of from 4 to 300 K has been performed for the first time. Different samples of the best "reflective" metals, such as silver, copper, gold, aluminum, and beryllium, have been investigated. These data are of interest for designing antenna systems with cooled mirrors in order to achieve the highest possible sensitivity of the receivers. Thus, based on these studies, the concept of covering all the cryogenically cooled reflectors of Millimetron with gold as the most stable and reproducible reflective material was adopted.

The experimental data were compared with the calculations based on the simplified model. As a result, it was found that the model describes well in general the qualitative dependence of the reflection loss on temperature, and in some cases (highly pure copper after the hydrogen annealing), the quantitative description can be considered satisfactory. At the same time, the character of variation in the frequency dependence in this temperature range (Fig. 13), as well as a significant quantitative difference between the experimental points and the calculation results for pure aluminum (Fig. 10), gold (Fig. 12), and silver (Fig. 14) indicate the need for more sophisticated models to determine the reflectivity of the real samples in the region of the anomalous skin effect. Such models should take into account many factors: 1) the difference between the Fermi surface and a sphere; 2) atomic structure of the sample surface (type of the crystal lattice, its orientation, whether the sample is a polycrystal); and 3) the effect of impurities and defects. Accurate calculation of the impact of all these factors on the reflectance is an extremely difficult task. Therefore, high-precision experimental data are the most reliable source of information.

Acknowledgment

The authors would like to thank Dr. V. Kurin for an informal review of this paper.

References

[1] T. P. McKenna, J. A. Nanzer, and T. R. Clark, "Photonic beamsteering of a millimeter-wave array with 10-Gb/s data transmission," *IEEE Photon. Technol. Lett.*, vol. 26, no. 14, pp. 1407–1410, Jul. 2014.

[2] R. V. Leslie and D. H. Staelin, "NPOESS aircraft sounder testbed-microwave: Observations of clouds and precipitation at 54, 118, 183, and 425 GHz," *IEEE Trans. Geosci. Remote Sens.*, vol. 42, no. 10, pp. 2240–2247, Oct. 2004.

[3] *The MILLIMETRON Site (Astro Space Center LPI 2016).* [Online]. Available: http://millimetron.ru/index.php/en/

[4] *The Scientific Programme of Planck (Bluebook). (ESA-SCI(2005)1).* [Online]. Available: http://www.cosmos.esa.int/web/planck/publications #PlanckProgramme

[5] *COrE. Cosmic Origins Explorer. A White Paper*. [Online]. Available: http://www.core-mission.org/documents/white_paper.pdf

[6] K. van't Klooster, S. E. Myasnikova, V. V. Parshin, and W. Kasparek, "Results of reflection loss measurements of sample material for radio astronomy telescope antenna for Planck project," in *Proc. 14th CriMiCo Conf.*, Sevastopol, Ukraine, 2004, pp. 753–755.

[7] V. V. Parshin, K. van't Klooster, and E. A. Serov, "Antenna reflectors reflectivity at 100-350 GHz and 80 K," in *Proc. 30th ESA Antenna Workshop*, Noordwijk, The Netherlands, 2008, pp. 353–357.

[8] V. V. Parshin, E. A. Serov, G. M. Bubnov, V. F. Vdovin, M. A. Koshelev, and M. Y. Tretyakov, "Cryogenic resonator complex," *Radiophys. Quantum Electron.*, vol. 56, nos. 8–9, pp. 554–560, Jan. 2014.

[9] A. A. Abrikosov, *Fundamentals of the Theory of Metals*. Oxford, U.K.: Elsevier, 1988.

[10] E. M. Lifshitz and L. P. Pitaevskii, "Metals," in *Physical Kinetics: Course of Theoretical Physics*, vol. 10. Oxford, U.K.: Elsevier, 2008.

[11] G. E. H. Reuter and E. H. Sondheimer, "The theory of the anomalous skin effect in metals," *Proc. Roy. Soc. A*, vol. 195, no. 1042, pp. 336–364, Dec. 1948.

[12] R. B. Dingle, "The anomalous skin effect and the reflectivity of metals I," *Physica*, vol. 19, nos. 1–2, pp. 311–347, 1953.

[13] V. V. Parshin and E. A. Serov, "Precise resonator methods investigation of dielectrics and metals at 40 GHz–500 GHz frequency range and in 4 K–900 K temperature interval," in *Proc. Global Symp. Millim. Waves (GSMM)*, Espoo, Finland, Jun. 2016, pp. 1–4.

[14] V. L. Ginzburg and G. P. Motulevich, "Optical characteristics of metals," (in Russian) *Usp. Fiz. Nauk*, vol. 55, no. 4, pp. 469–534, Apr. 1955.

[15] J. Bardeen, "Electrical conductivity of metals," *J. Appl. Phys.*, vol. 11, no. 2, pp. 88–111, 1940.

[16] A. F. Krupnov, M. Y. Tretyakov, V. V. Parshin, V. N. Shanin, and S. E. Myasnikova, "Modern millimeter-wave resonator spectroscopy of broad lines," *J. Molecular Spectrosc.*, vol. 202, no. 1, pp. 107–115, Jul. 2000.

[17] M. Y. Tretyakov, A. F. Krupnov, M. A. Koshelev, D. S. Makarov, E. A. Serov, and V. V. Parshin, "Resonator spectrometer for precise broadband investigations of atmospheric absorption in discrete lines and water vapor related continuum in millimeter wave range," *Rev. Sci. Instrum.*, vol. 80, no. 9, p. 093106, Sep. 2009.

[18] V. V. Parshin, M. Y. Tretyakov, M. A. Koshelev, and E. A. Serov, "Modern resonator spectroscopy at submillimeter wavelengths," *IEEE Sensors J.*, vol. 13, no. 1, pp. 18–23, Jan. 2013.

[19] V. Parshin, E. Serov, C. G. M. K. van't Klooster, and P. Noschese, "Resonator technique for reflectivity measurements. Results for measurements at high temperatures," in *Proc. 31st ESA Antenna Workshop*, Noordwijk, The Netherlands, 2009, pp. 593–600.

[20] I. S. Grigorieva and E. Z. Meilikhova, Eds., *Physical Quantities, Handbook* (in Russian). Moscow, Russia: Energoatomizdat, 1991, p. 438.

[21] W. Espe, "Werkstoffkunde der Hochvakuumtechnik," in *Metalle und Metallisch Leitende Werkstoffe*. Berlin, Germany: Deutscher Verlag der Wissenschaften, 1959.

[22] V. A. Kutovoy and A. M. Yegorov, "Design concept of cryogenic accelerating structures of a copper accelerator," *Tech. Phys.*, vol. 53, no. 3, pp. 371–375, Mar. 2008.

[23] S. Inagaki, E. Ezura, J.-F. Liu, and H. Nakanishi, "Thermal expansion and microwave surface reactance of copper from the normal to anomalous skin effect region," *J. Appl. Phys.*, vol. 82, no. 11, pp. 5401–5410, Dec. 1997.

[24] *Materials of the Millimetron*. (Feb. 12, 2015). [Online]. Available: http://specport.asc.rssi.ru/index.php/en/space-telescope/design/materials

Evgeny A. Serov, photograph and biography not available at the time of publication.

Vladimir V. Parshin, photograph and biography not available at the time of publication.

Grigoriy M. Bubnov, photograph and biography not available at the time of publication.